

# Applying Convolutional Neural Networks for the Source Reconstruction

He Ming Yao<sup>1</sup>, Wei E. I. Sha<sup>2</sup>, and Li Jun Jiang<sup>1, \*</sup>

**Abstract**—This paper proposes a novel source reconstruction method (SRM) based on the convolutional neural network algorithm. The conventional SRM method usually requires the scattered field data oversampled compared to that of target object grids. To achieve higher accuracy, the conventional SRM numerical system is highly singular. To overcome these difficulties, we model the equivalent source reconstruction process using the machine learning. The equivalent sources of the target are constructed by a convolutional neural networks (ConvNets). It allows us to employ less scattered field samples or radar cross section (RCS) data. And the ill-conditioned numerical system is effectively avoided. Numerical examples are provided to demonstrate the validity and accuracy of the proposed approach. Comparison with the traditional NN is also benchmarked. We further expand the proposed method into the direction of arrival (DOA) estimation to demonstrate the generality of the proposed procedure.

## 1. INTRODUCTION

In past two decades, the source reconstruction method (SRM) has been an attractive method to retrieve equivalent source distributions of target objects from the near or far field measurements [1, 2]. As a representative electromagnetic inverse scattered problem, SRM can employ integral equations to implement far field (FF) to near field (NF) transformation [3, 4]. From the scattered field in the observation domain, the distribution of the sources on an object can be approximated through SRM. The reconstructed sources can provide many helpful applications, such as source error test, hot-spot identification, and NF to FF transformations [3–5]. A large number of reconstruction algorithms have been proposed for SRM and related purposes, such as Born approximation method [6, 7], Bayesian probability method [8, 9], compressive sensing [10], and other deterministic algorithms [11, 12]. The source reconstruction method could be implemented through integral equation method and MoM [6–9]. It can also be carried out through other numerical or experimental processes as long as the needed training data could be generated. However, all these conventional approaches encounter solving singular numerical systems, which make SRM a complicated computational challenge [2, 6].

Employing machine learning (ML) in advanced computational electromagnetics and relevant applications were initiated long time ago [13–16]. Artificial neural networks (ANN) have been proposed for array synthesis [17], source reconstruction [18], NF to FF transformation [19], etc. Due to the recent blooming learning technologies, convolutional neural networks (ConvNets) [20, 21] have become one of the most important new methods in deep learning applications. For example, ConvNet has been widely used in imaging processes [22, 23].

In this paper, we propose to employ the power of ConvNet for the source reconstruction process. The advantages of the proposed method are: (1) the proposed ConvNet model allows calculation

---

*Received 29 August 2018, Accepted 31 October 2018, Scheduled 27 November 2018*

\* Corresponding author: Li Jun Jiang (jianglj@hku.hk).

<sup>1</sup> Department of Electrical and Electronic Engineering, The University of Hong Kong, Hong Kong, China. <sup>2</sup> College of Information Science & Electronic Engineering, Zhejiang University, Hangzhou, China.

using much fewer field samples than the conventional SRM; (2) without inverse solving, the proposed method avoids handling a singular numerical system; (3) the proposed ConvNet approach can make further field information to do reconstruction; (4) the proposed method has satisfactory accuracy and superior performance over traditional neural networks [17–19]. Compared to traditional neural networks (NNs) [17–19, 24], ConvNet can more efficiently map the relations between inputs and outputs mainly by convolutional layer and activation layer [20, 21]. It does not need very large number of neural units to handle problems such as source reconstruction. To demonstrate this difference, the SRM performance comparison between ConvNet and traditional NN is provided in Section 3.

The paper is organized as follows. In Section 2, the source reconstruction formulation is briefly reviewed, followed by a description of the ConvNets structure. Then, the proposed ConvNet method for solving source reconstruction problems is proposed. In Section 3, numerical examples are provided to present the validity and precision of the proposed method, which are also compared with the results obtained by different interpolation methods [25]. Finally, the conclusion is shown in Section 4.

## 2. THEORY AND FORMULATION

### 2.1. Problem Formulation

We use a representative 2D equivalent current density reconstruction, as shown in Figure 1, to demonstrate the procedures of our methodology. Here, we want to emphasize that our work is not done on non-radiating sources [26]. In Figure 1,  $D_{obj}$  is a dielectric area, denoting the domain of interest. It is divided into  $n = 1, 2, \dots, N$  patches. The transverse magnetic (TM) incidence plane wave is denoted as  $\mathbf{E}^{in}$ . The scattered field  $\mathbf{E}^s$  in  $z$  direction can be represented by the  $z$  direction current density as:

$$E^s(\mathbf{r}) = -j\omega\mu_0 \int g(\mathbf{r}, \mathbf{r}') J_s(\mathbf{r}') d\mathbf{r}' \quad (1)$$

where  $g(\mathbf{r}, \mathbf{r}')$  is the scalar Green's function. For TM wave, it can be defined as  $g(\mathbf{r}, \mathbf{r}') = -\frac{j}{4} H_0^{(2)}(k_0 |\mathbf{r} - \mathbf{r}'|)$ .  $H_0^{(2)}$  stands for the second-kind Hankel function of zero<sup>th</sup> order.  $\mathbf{r} = (xy)$  and  $\mathbf{r}' = (x', y')$  are the field and source points, respectively.  $\mathbf{J}_s$  is the equivalent current density on the target object  $D_{obj}$ .

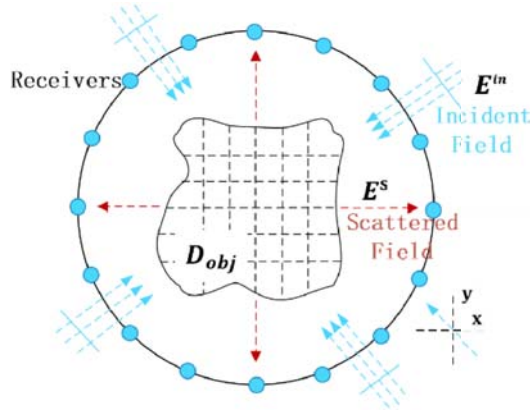


**Figure 1.** Schematic of the scattering of TM wave from a dielectric region  $D_{obj}$ .

Based on the Lippmann-Schwinger equation [27], the relationship between the incident electrical field  $\mathbf{E}^{in}$  and equivalent current density distribution  $\mathbf{J}_s$  on  $D_{obj}$  is:

$$E^{in}(\mathbf{r}) - j\omega\mu_0 \int g(\mathbf{r}, \mathbf{r}') J_s(\mathbf{r}') dr' = \frac{J_s(\mathbf{r})}{j\omega\epsilon_0(\epsilon_r - 1)} \quad (2)$$

where  $\epsilon_0$  and  $\mu_0$  are the vacuum permittivity and permeability, and  $\epsilon_r$  is the relative permittivity of  $D_{obj}$ .

It has been widely accepted that the property of object can be characterized by its equivalent current density distribution  $\mathbf{J}_s$ . For different incident angles  $\beta_l$  of  $\mathbf{E}^{in}$  ( $l = 1 \dots L$ ) and different receivers in the far field at measurement angles  $\varphi_m$  ( $m = 1 \dots M$ ), the relationship between the scattered field  $\mathbf{E}^s$  and equivalent current density  $\mathbf{J}_s$  is:

$$E^s(\varphi_m, \beta_l) = -j\omega\mu_0 \sum_{n=1}^N g(\varphi_m, \mathbf{r}'_n) J_{s,n}^{\beta_l} A_n \quad (3)$$

where  $A_n$  is the equivalent area of  $n^{\text{th}}$  divided  $D_{\text{obj}}$  fragment, and  $J_{s,n}^{\beta_l}$  is the equivalent current density on the  $n^{\text{th}}$  piece with the incident field angle  $\beta_l$ .

For conventional reconstruction methods, we aim to use  $E^s(\varphi_m, \beta_l)$  to obtain  $J_{s,n}^{\beta_l}$ . However, in the conventional process, we have to use large number of  $\varphi_m$  to retrieve  $J_{s,n}^{\beta_l}$ , which could be ill-conditioned [28]. Hence, the expensive calculation cost and relatively low accuracy are the bothering problem for SRM. ConvNet provides a possible new approach to solve the problem with smaller  $M$ . According to Eq. (3), we rewrite the process of solving  $\mathbf{J}_s$  matrix vector in a simplified form as Eq. (4):

$$\mathbf{J}_s = \Gamma(\mathbf{E}^s) \quad (4)$$

where for each  $\beta_l$ ,  $\mathbf{E}^s = [E^s(\varphi_1, \beta_l), \dots, E^s(\varphi_M, \beta_l)]$  and  $\mathbf{J}_s = [J_{s,1}^{\beta_l}, \dots, J_{s,n}^{\beta_l}, \dots, J_{s,N}^{\beta_l}]$ . The mapping  $\Gamma$  represents the equivalent source reconstruction.

### 2.2. Integration of ConvNet and Source Reconstruction

A ConvNets [20, 21] consists of four stacked layers: input layers, convolutional layers, pooling layers and fully-connected layers. In this paper, we utilize these typical layers to form our convolutional neural network model to reconstruct equivalent source for a process in Equation (4).

The internal architecture of our ConvNet is shown in Figure 2. The inputs are  $\mathbf{E}^s$  of each size  $2M \times 1$  with real part  $M \times 1$  and imagery part  $M \times 1$ , illuminated from  $L$  groups of incident field. Here, if we use RCS value of scattering field as input data, the size of each input becomes  $M \times 1$ . The convolutional layer and activation layer unit operates to capture features of input.  $f$  filters (kernel) in convolutional layer have size of  $K \times 1$  due to 1D input. Convolutional layer number, kernel number  $f$ , its size  $K$ , and the stride for kernel are adjusted according to a specific application scenario. Then, this convolutional layer and activation layer unit feeds into a final fully-connected layer, which produces the reconstructed source  $\mathbf{J}_s$  with size  $2N$  as real and imagery parts or with size  $N$  as its modulus. This final output is the output value of the ConvNet. It is used to compute the mean-squared error between the true label and the predicted label, referred to as the loss.

Our method is benchmarked in Matlab 2017b with Deep Learning Toolbox [29]. The mean-squared error loss function is optimized by stochastic gradient descent. The learning rate, chosen as 0.01, is

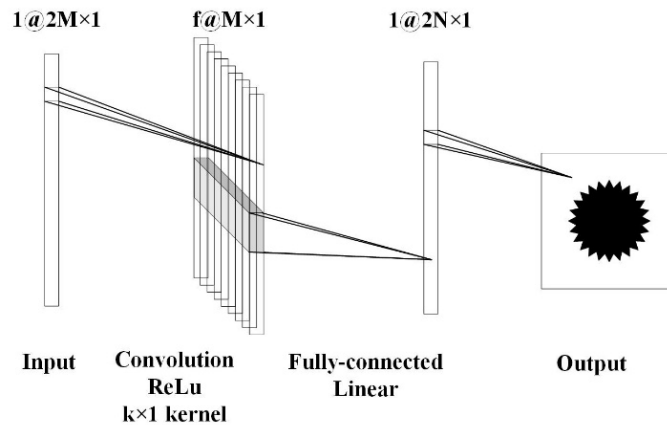


Figure 2. ConvNet architecture for the source reconstruction.

the hyper-parameter in our model. We can control training error by declining the learning rate. The training is done by Full batch. L2 regularization is applied to prevent over-fitting and improve prediction accuracy [30]. If input  $\mathbf{E}^s$  is smooth, we tend to choose smaller convolutional layer number and kernel number, and larger kernel size and stride to efficiently capture features of input because less fluctuation means narrower bandwidth with limited field information and limited critical features. Besides, if the stride is larger than 1, this convolutional layer acts as reducing layer to compress ‘resolution’ of ‘image’. Moreover, for simplicity, we do not use pooling layers in our ConvNet structure. Moreover, there is no requirement to manually select features, which makes the proposed ConvNet approach a featureless-learning one. The computational complexity of our ConvNet is  $O(DMKf^2) + O(MN)$ , where  $O(DMKf^2)$  is the computational complexity of all convolutional unit, and  $O(MN)$  is the computational complexity of the last fully-connected regression layer.  $N$  (square of grid size) is the size of output  $\mathbf{J}_s$ , and  $D$  is the number of convolutional units [31]. Normally, we control the number of convolutional units and choose small kernel number and size. Thus, we have  $N \gg DKf^2$  for the ConvNet, and the computational complexity of the ConvNet is  $O(MN)$ . According to our experience, even when we choose small number of receivers, meaning  $N \gg M$ , the ConvNet can still offer satisfactory result. In this way, the computational complexity of the ConvNet is approximated to  $O(N)$ .

To be specific, we use the ConvNet  $F$  to replace the relation  $\Gamma$  in Eq. (4). We choose  $\mathbf{E}^s$  as the input of the structure and  $\mathbf{J}_s$  as output of the structure.

$$\begin{cases} \mathbf{Y} = F(\mathbf{X}; \Theta) \\ \mathbf{X} = \mathbf{E}^s \\ \mathbf{Y} = \mathbf{J}_s \end{cases} \quad (5)$$

where  $\mathbf{E}^s$  and  $\mathbf{J}_s$  in different incident angles  $\beta_l$  act as training data, and we have  $L$  groups of input and output of ConvNet.  $\Theta$  is the parameters of the ConvNet (weights and biases).

The training of  $F$  is done by using known  $\mathbf{J}_s$  under different incident waves and its resultant  $\mathbf{E}^s$  to form training data set for the ConvNet. Based on the trained ConvNet, we can then reconstruct  $\mathbf{J}_s$  illuminated by new incident waves with less complexity and more accuracy. The performance of the ConvNet is discussed in the following sections.

### 3. NUMERICAL RESULTS

We use several numerical examples and application scenarios to demonstrate the proposed source reconstruction method.

#### 3.1. Reconstruction on Symmetrical Object

We begin from a 2D dielectric cylinder, which means that  $D_{\text{obj}}$  is rotationally symmetric. Using the measured RCS, we can get  $\mathbf{J}_s$  from the trained ConvNet.

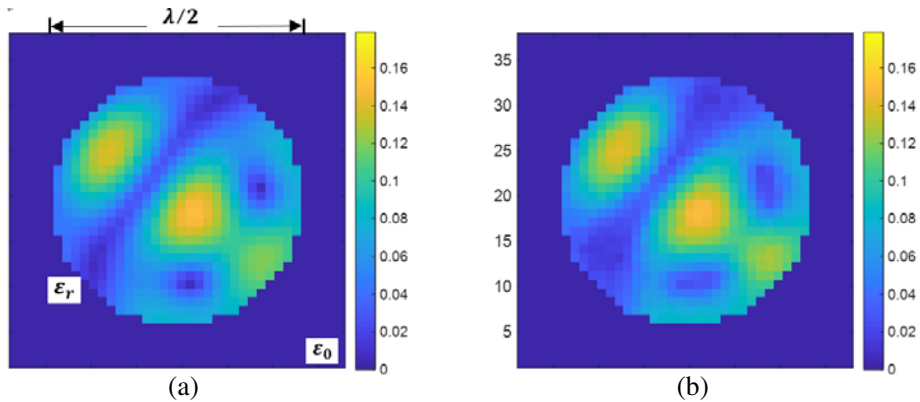


**Figure 3.** ConvNet performance. (a) Known accurate current distribution. (b) Current distribution computed from the ConvNet prediction based on the measured RCS.

In Figure 3, the wavelength  $\lambda$  of incident  $TM_z$  wave is 1 meter; the permittivity of dielectric object  $\epsilon_r$  is 8; and its radius is  $\lambda/4$ . The grid size of current distribution  $\mathbf{J}_s$  is  $38 \times 38$ , thus  $N = 1444$ . The RCS data are collected from only  $M = 12$  different angles as input of training data. We just use  $L = 15$  different incident angles ( $\beta = 0^\circ, 24^\circ, \dots, 336^\circ$ ) to stimulate the object to get the training data. Then, we use a new incident angle ( $\beta = 36^\circ$ ) of wave to get different RCSs, which is used as the input of the trained ConvNet to predict the new distribution of  $\mathbf{J}_s$ . The comparisons of the accurate numerical results and ConvNet prediction results are shown in Figure 3. The average relative error between them is less than 3%.

The ConvNet adopted in this model has one convolution and activation unit, 5 kernels with the size  $3 \times 1$  for each of them, and the stride 2. Here we should emphasize that all those parameters might not ensure the best performance of ConvNet, and they still have potentials to be optimized.

### 3.2. Reconstruction on Asymmetric Object

In this section, we test the performance of ConvNet for an asymmetric  $D_{obj}$ , a L shape object. To demonstrate the advantage of ConvNet, we compare its performance with two interpolation methods [25], the nearest interpolation and spectral interpolation, and with traditional Back Propagation Neural Network (BPNN) [24].

In this benchmark, the wavelength  $\lambda$  of incident  $TM_z$  wave is 1 meter. The relative permittivity of dielectric object  $\epsilon_r$  is 8. Its outer length  $a$  is  $\lambda/2$  with the inner length  $b$  equal to  $3\lambda/8$  (See Figure 4(a)). The grid size of current distribution  $\mathbf{J}_s$  is  $24 \times 24$ . Here we use both real and imaginary parts of  $\mathbf{J}_s$  to form a full vector with the length  $N = 1152$ . The  $\mathbf{E}^s$  made of real and imaginary parts of scattering fields are collected from 10 different angles as the input of training data, and  $M = 20$ . We only use 6 different incident angles ( $\beta = 0^\circ, 60^\circ, \dots, 300^\circ$ ) of  $\mathbf{E}^{in}$  to stimulate the object to get training data. For the spectral interpolation method as a reference, we use two-times zero-padding and fast Fourier transform to interpolate each grid of the current distribution of the area with  $24 \times 24$  grids. Besides,

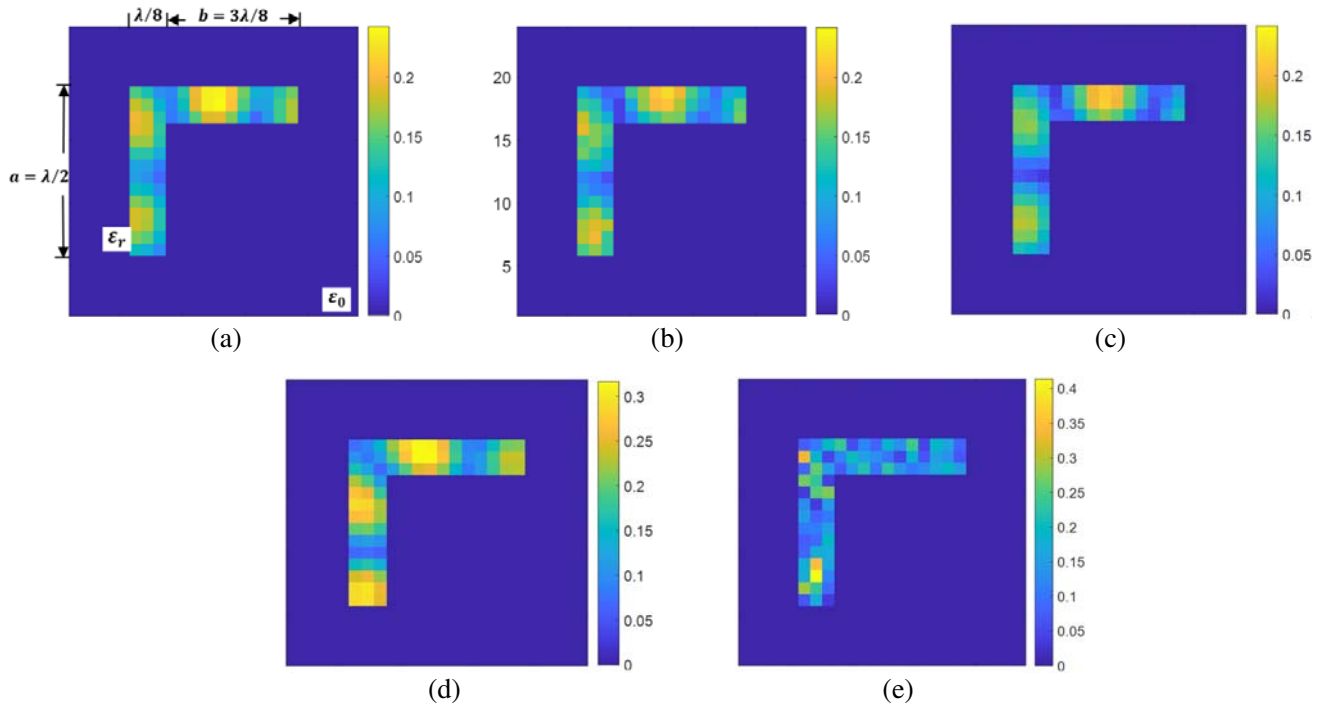


**Figure 4.** Performance of different approaches on L object for  $\beta = 210$  degree. (a) Known accurate numerical current distribution. (b) Current distribution calculated from the ConvNet prediction. (c) Current distribution calculated from spectral interpolation. (d) Current distribution calculated from the nearest interpolation. (e) Current distribution calculated from traditional BPNN.

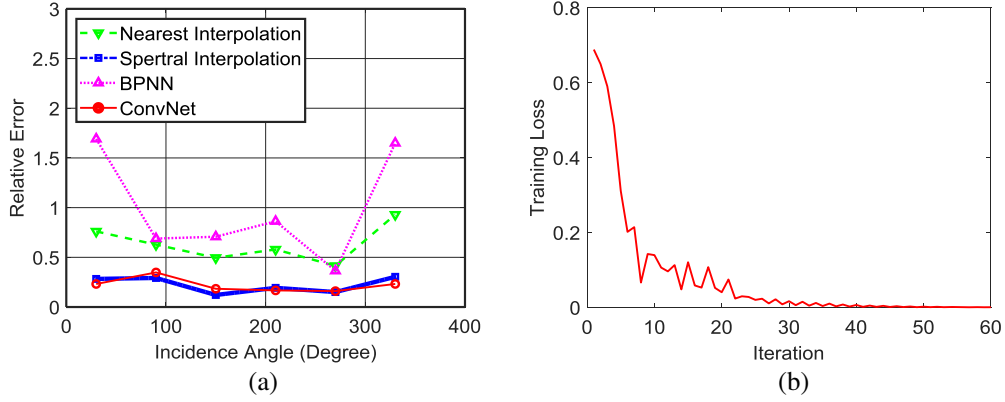


**Figure 5.** (a) Relative error comparison between ConvNet, BPNN, the nearest interpolation and spectral interpolation on different incident angles. (b) Training loss of ConvNet.

we also use traditional Back Propagation Neural Network (BPNN) to reconstruct the source [24], of which the training data are also  $\mathbf{E}^s$  as input and  $\mathbf{J}_s$  as output. Traditional NNs usually depend on neural unit and hidden layer to fit the relationship between input and output, and have to make use of a large number of neural units to handle source reconstruction problem with the relatively complicated relationship between input and output [17, 19]. The structure of BPNN has three layers: input, hidden-layer and output layer. There are 20 hidden-layer units of hyperbolic tangent basis function. This BPNN is implemented using Matlab 2017b with Deep Learning Toolbox [29].

We use a new incident angle  $\beta = 210^\circ$  to obtain a different set of  $\mathbf{J}_s$  and  $\mathbf{E}^s$  from the L shape object. Then, we utilize  $\mathbf{E}^s$  as the input of the trained ConvNet to predict  $\mathbf{J}_s$ . Figure 4 shows the prediction result of ConvNet and traditional BPNN and two interpolation results. From Figure 4 and Figure 5, we can clearly see that the ConvNet and spectral interpolation have comparable precision with accurate numerical values, while the nearest interpolation has more errors in retrieving the equivalent source distribution. However, the traditional BPNN nearly fails to predict reconstructed source or provide meaningful information, shown in Figure 4(e). Meanwhile, the computational complexity of our ConvNet is  $O(MN)$ , where  $M$  is the size of the input  $\mathbf{E}^s$ , and  $N$  is the size of the output  $\mathbf{J}_s$ . For this example,  $N \gg M$ . Thus, the computational complexity of the ConvNet is  $O(N)$ , which is the same as the nearest interpolation method and lower than the spectral interpolation with the complexity of  $O(N \log N)$ . For the ConvNet in Figure 4(b), though merely one convolution and activation unit are applied, it still shows surprisingly excellent performance, presented in Figure 4 and Figure 5.

In Figure 5(a), we utilize five incident angles ( $\beta = 30^\circ, 90^\circ \dots 330^\circ$ ) to stimulate the object. The following relative error function in Eq. (6) is applied to evaluate the accuracy of our ConvNet and two interpolation approaches:

$$e = \frac{\| \mathbf{J}_{\mathbf{S},\text{SRM}} - \mathbf{J}_{\mathbf{S},\text{acc}} \|}{\| \mathbf{J}_{\mathbf{S},\text{acc}} \|} \quad (6)$$

where  $\mathbf{J}_{\mathbf{S},\text{SRM}}$  is the current density computed from source reconstruction methods, and  $\mathbf{J}_{\mathbf{S},\text{acc}}$  is the accurate current density distribution.

We can see that the ConvNet has the same small error (about 0.2) and thus the same accuracy as the spectral interpolation, both of which are much better than the nearest interpolation (about 0.5). Besides, from Figure 5(b), we can see that the training loss of ConvNet rapidly decreases and that our ConvNet successfully captures the features of  $\mathbf{E}^s$  and maps them to  $\mathbf{J}_s$ . Moreover, in this application scenario, least square error (LSE) method fails to reconstruct  $\mathbf{J}_s$ , because  $N \gg M$  and  $\mathbf{J}_s$  cannot be computed by underdetermined situation.

### 3.3. Direction of Arrival Estimation

To expand the application of our ConvNet model, we use it to do direction of arrival (DOA) estimation on the angle of incidence wave. Conventional DOA needs complex receiver and analysis tools [32], such

as complex antenna array, and complicated algorithms, such as MUSIC [33]. By ConvNet model, DOA estimation could be done by merely a small number of known  $\mathbf{E}^s$  and incidence cases. We firstly choose one target object  $D_{\text{obj}}$  as a medium to map relationship between scattered field  $\mathbf{E}^s$  and incident angle  $\beta_l$ . We still utilize  $\mathbf{E}^s$  as the input of ConvNet, but use the incidence angle of electromagnetic wave  $\beta_l$  as output of ConvNet. By this trained ConvNet, we can also predict the incident angle. The performance of our model is shown in Figure 6. We here use the L shape in Section B as medium target object  $D_{\text{obj}}$ . Parameters of ConvNet in this example are the same as those in the numerical example above.

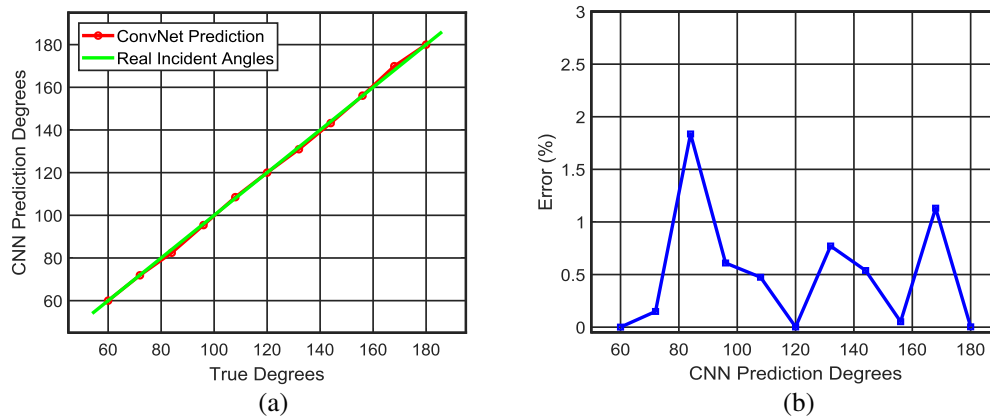


**Figure 6.** DOA results from ConvNet. (a) Comparison between real incident angles and ConvNet prediction results. (b) Error of ConvNet prediction results.

From Figure 6, we can see that the ConvNet can accurately predict the incident angle of wave  $\beta_l$ , and in most cases, the error of ConvNet prediction results can be controlled below 1.5%.

#### 4. CONCLUSION

In this paper, we propose a new source reconstruction method using the ConvNets model from machine learning. The scattered fields due to incident waves from different incident angles are used as the input training data to the ConvNets. The induced current distributions are used as the output data. After the training, ConvNets serves as the SRM engine to reconstruct the equivalent sources efficiently. Because of the merit of ConvNets, the newly proposed approach achieves better performance on the source reconstruction problem. Symmetric and asymmetric objects are used to demonstrate the feasibility and accuracy of the retrieved source distribution. We also compare the reconstructed source distribution from the proposed ConvNet model with that from traditional neural networks, and from spectral interpolation and the nearest interpolation methods to show the validity and advantages of our model. The ConvNets model is further extended to solve the direction of arrival estimation. Our work offers a new way to leverage machine learning approaches for source reconstruction applications.

#### ACKNOWLEDGMENT

This work was supported in part by the Research Grants Council of Hong Kong (GRF 17209918, GRF 17207114 and GRF 17210815), AOARD FA2386-17-1-0010, NSFC 61271158, HKU Seed Fund 104005008, and Hong Kong UGC AoE/P-04/08.

#### REFERENCES

1. Araque Quijano, J. L. and G. Vecchi, "Field and source equivalence in source reconstruction on 3D surfaces," *Progress In Electromagnetics Research*, Vol. 103, 67–100, 2010.

2. Persson, K. and M. Gustason, "Reconstruction of equivalent currents using a near-field data transformation-with radome applications," *Progress In Electromagnetics Research*, Vol. 54, 179–198, 2005.
3. Sarkar, T. K., P. Petre, A. Taaghool, and R. F. Harrington, "An alternative spherical near field to far field transformation," *Progress In Electromagnetics Research*, Vol. 16, 269–284, 1997.
4. Li, P. and L. J. Jiang, "The far field transformation for the antenna modeling based on spherical electric field measurements," *Progress In Electromagnetics Research*, Vol. 123, 243–261, 2012.
5. Alvarez, Y., F. Las-Heras, and M. R. Pino, "On the comparison between the spherical wave expansion and the sources reconstruction method," *IEEE Trans. Antennas Propag.*, Vol. 56, No. 10, 3337–3341, 2008.
6. Crocco, L. and M. D'Urso, "The contrast source-extended Born model for 2D subsurface scattering problems," *Progress In Electromagnetics Research B*, Vol. 17, 343–359, 2009.
7. Chew, W. C. and Y. M. Wang, "Reconstruction of two-dimensional permittivity distribution using the distorted Born iterative method," *IEEE Trans. Med. Imag.*, Vol. 9, No. 2, 218–225, 1990.
8. Caorsi, S., G. L. Gragnani, S. Medicina, M. Pastorino, and G. A. Pinto, "A Gibbs random field-based active electromagnetic method for noninvasive diagnostics in biomedical applications," *Radio Sci.*, Vol. 30, 291–301, 1995.
9. Yu, Y. and L. Carin, "Three-dimensional Bayesian inversion with application to subsurface sensing," *IEEE Trans. Geosci. Remote Sens.*, Vol. 45, No. 5, 1258–1270, 2007.
10. Chen, M. S., F. L. Liu, H. M. Du, and X. L. Wu, "Compressive sensing for fast analysis of wide-angle monostatic scattering problems," *IEEE Antennas Wireless Propag. Lett.*, Vol. 10, 1243–1246, 2011.
11. Kleinman, R. E. and P. M. van den Berg, "Two-dimensional location and shape reconstruction," *Radio Sci.*, Vol. 29, 1157–1169, 1994.
12. Sun, S., B. J. Kooij, and A. Yarovoy, "Linearized three-dimensional electromagnetic contrast source inversion and its applications to half-space configurations," *IEEE Trans. Geosci. Remote Sens.*, Vol. 55, No. 6, 3475–3487, 2017.
13. Shan, T., X. W. Dang, M. K. Li, F. Yang, S. H. Xu, and J. Wu, "Study on a Poisson's equation solver based on deep learning technique", arXiv:1712.05559, 2017.
14. Yao, H., L. Jiang, and Y. Qin, "Machine learning based method of moments (ML-MoM)," *Proceedings of 2017 IEEE International Symposium on Antennas and Propagation & USNC/URSI National Radio Science Meeting*, San Diego, USA, July 2017.
15. Shan, T., X. W. Dang, M. K. Li, F. Yang, S. H. Xu, and J. Wu, "Study on a 3D Poisson's equation solver based on deep learning technique," *Proceedings of IEEE Int. Conf. Computational Electromagnetics*, Chengdu, China, March 2018.
16. Zhang, H. H. and R. S. Chen, "Coherent processing and superresolution technique of multi-band radar data based on fast sparse bayesian learning algorithm," *IEEE Trans. Antennas Propag.*, Vol. 62, No. 12, 6217–6227, 2014.
17. Ayestarn, R. G., F. L. Heras, and L. F. Herran, "High accuracy neural network-based array synthesis including element coupling," *IEEE Antennas Wireless Propag. Lett.*, Vol. 5, No. 1, 45–48, 2006.
18. Ayestarn, R. G. and F. L. Heras, "Neural networks and equivalent source reconstruction for real antenna array synthesis," *Electron. Lett.* Vol. 39, No. 13, 956–958, 2003.
19. Ayestarn, R. G. and F. L. Heras, "Near filed to far field transformation using neural networks and source reconstruction," *Journal of Electromagnetic Waves and Applications*, Vol. 20, No. 15, 2201–2213, 2006.
20. Krizhevsky, A., I. Sutskever, and G. Hinton, "ImageNet classification with deep convolutional neural networks," *Proc. Neural Information and Processing Systems*, 2012.
21. Zhang, Y., D. Zhao, J. Sun, G. Zou, and W. Li, "Adaptive convolutional neural network and its application in face recognition," *Neural Processing Letters*, Vol. 43, No. 2, 389–399, 2015.

22. Dong, C., C. Loy, K. He, and X. Tang, "Image super-resolution using deep convolutional networks," *IEEE Transactions on Pattern Analysis and Machine Intelligence*, Vol. 38, No. 2, 295–307, 2016.
23. Sahiner, B., H.-P. Chan, N. Petrick, D. Wei, M. Helvie, D. Adler, and M. Goodsitt, "Classification of mass and normal breast tissue: a convolution neural network classifier with spatial domain and texture images," *IEEE Transactions on Medical Imaging*, Vol. 15, No. 5, 598–610, 1996.
24. Hornik, K., M. Stinchcombe, and H. White, "Multilayer feedforward networks are universal approximators," *Neural Netw.*, Vol. 2, No. 5, 359–366, 1989.
25. Hoang, N., "On node distributions for interpolation and spectral methods," *Mathematics of Computation*, Vol. 85, No. 298, 667–692, 2015.
26. Labate, G., Matekovits, L. and Podilchak, S., "A methodology for translating non-radiating sources in design parameters of cloaking devices," *Proceedings of 2016 IEEE International Symposium on Antennas and Propagation (APSURSI)*, Fajardo, Puerto Rico, June 2016.
27. Fiddy, M. A. and R. S. Ritter, *Introduction to Imaging from Scattered Fields*, CRC Press, 2014.
28. Hansen, P., *Discrete Inverse Problems: Insight and Algorithms*, SIAM, Philadelphia, PA, USA, 2010.
29. Kim, P., *MATLAB Deep Learning*, Apress, 2017.
30. Ng, A. Y., "Feature Selection L1 vs. L2 Regularization and Rotational Invariance," *Proceedings of 21st Int'l Conf. Machine Learning*, 78–86, 2004.
31. Cong, J. and B. Xiao, "Minimizing computation in convolutional neural networks," *Proceedings of Int. Conf. Artif. Neural Netw.*, 281–290, 2014.
32. Tan, Z., Y. C. Eldar, and A. Nehorai, "Direction of arrival estimation using co-prime arrays: A super resolution viewpoint," *IEEE Trans. Signal Process.*, Vol. 62, No. 21, 5565–5576, 2014.
33. Zhang, X., L. Y. Xu, L. Xu, and D. Xu, "Direction of departure (DOD) and direction of arrival (DOA) estimation in MIMO radar with reduced-dimension MUSIC," *IEEE Commun. Lett.*, Vol. 14, No. 12, 1161–1163, 2010.